Lawrence Berkeley National Laboratory
LBL Publications

Title
Atomic layer deposition for spacer defined double patterning of sub-10 nm titanium dioxide features

Permalink
https://escholarship.org/uc/item/2mq5j0t3

Journal
Nanotechnology, 29(40)

ISSN
0957-4484

Authors
Dallorto, Stefano
Staaks, Daniel
Schwartzberg, Adam
et al.

Publication Date
2018-10-05

DOI
10.1088/1361-6528/aad393

Peer reviewed

eScholarship.org Powered by the California Digital Library
University of California

Nanotechnology

PAPER

Atomic layer deposition for spacer defined double patterning of sub-10 nm titanium dioxide features

To cite this article: Stefano Dallorto *et al* 2018 *Nanotechnology* **29** 405302

View the article online for updates and enhancements.

IOP ebooks™

Bringing you innovative digital publishing with leading voices to create your essential collection of books in STEM research.

Start exploring the collection - download the first chapter of every title for free.

This content was downloaded from IP address 131.243.223.46 on 09/10/2018 at 17:15

IOP Publishing

Nanotechnology

Nanotechnology **29** (2018) 405302 (7pp)

https://doi.org/10.1088/1361-6528/aad393

Atomic layer deposition for spacer defined double patterning of sub-10 nm titanium dioxide features

Stefano Dallorto[1,2,3], Daniel Staaks[1,2,4], Adam Schwartzberg[1], XiaoMin Yang[4], Kim Y Lee[4], Ivo W Rangelow[2], Stefano Cabrini[1] and Deirdre L Olynick[1,5]

[1] Molecular Foundry, Lawrence Berkeley National Laboratory, Berkeley, CA 94720, United States of America
[2] Ilmenau University of Technology, Department of Micro-and Nanoel. Syst., D-98684, Germany
[3] Oxford Instruments, 300 Baker Avenue, Suite 150, Concord, MA 01742, United States of America
[4] Seagate Technology, 47010 Kato Road, Fremont, CA 94538, United States of America

E-mail: Deirdre.Olynick@ucsf.edu

Received 8 March 2018, revised 10 July 2018
Accepted for publication 16 July 2018
Published 27 July 2018

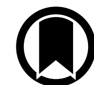

CrossMark

Abstract

The next generation of hard disk drive technology for data storage densities beyond 5 Tb/in^2 will require single-bit patterning of features with sub-10 nm dimensions by nanoimprint lithography. To address this challenge master templates are fabricated using pattern multiplication with atomic layer deposition (ALD). Sub-10 nm lithography requires a solid understanding of materials and their interactions. In this work we study two important oxide materials, silicon dioxide and titanium dioxide, as the pattern spacer and look at their interactions with carbon, chromium and silicon dioxide. We found that thermal titanium dioxide ALD allows for the conformal deposition of a spacer layer without damaging the carbon mandrel and eliminates the surface modification due to the reactivity of the metal–organic precursor. Finally, using self-assembled block copolymer lithography and thermal titanium dioxide spacer fabrication, we demonstrate pattern doubling with 7.5 nm half-pitch spacer features.

Supplementary material for this article is available online

Keywords: double patterning, bit patterned media, atomic layer deposition, sequential infiltration synthesis, template fabrication

(Some figures may appear in colour only in the online journal)

Introduction

The future of magnetic data storage beyond perpendicular recording will require replacing the conventional granular magnetic media with bit patterned media (BPM) [1, 2]. Lithographically defining the single bit is necessary to maintain the thermal stability needed for magnetic recording [3]. In order to reach storage density beyond 5 Tb/in^2, BPM demands isolated sub-10 nm feature sizes over a large area [4].

[5] Current address: University of California, San Francisco, San Francisco, CA 94143, United States of America

Current optical lithographies do not have the resolution to meet the critical dimension requirements [5]. Electron beam lithography has sub-10 nm resolution [6], but is a serial method with low-throughput [7]. Cross-nanoimprint lithography (NIL) [1, 8] on the other hand, allows for stitchless, high volume production and enables to pattern features at the single digit nanoscale [9, 10]. As UV curing is preferred over thermal curing [1, 8], the master template is usually fabricated from quartz substrates. Herein, we target fabricating master templates on quartz to meet BPM with an areal density greater than 5 Tb/in^2. This requires sub-10 nm half-pitch features to be patterned with single nanometer control. For these reasons a solid understanding

 © 2018 IOP Publishing Ltd Printed in the UK

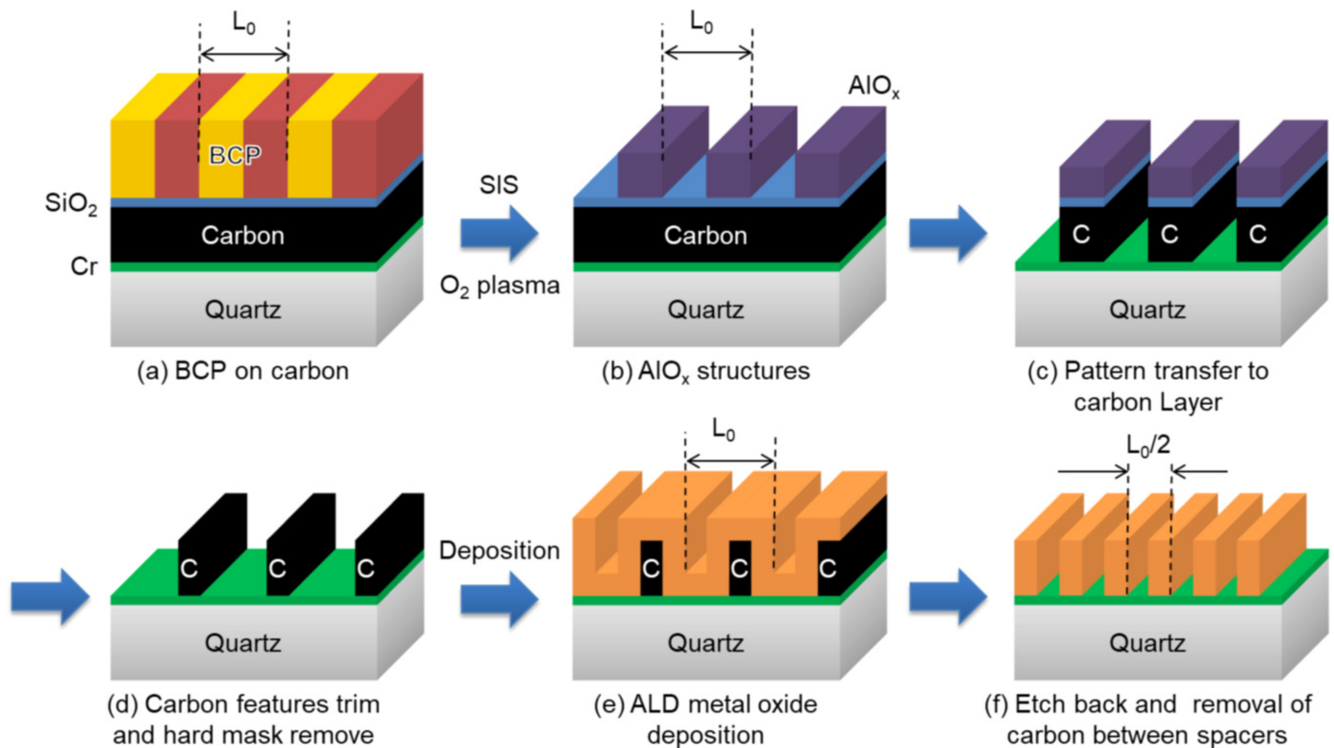

Figure 1. Line frequency doubling flow. (a) Initial PS-*b*-PMMA BCP pattern. (b) Sequential infiltration synthesis (SIS) of Al_xO_y using atomic layer deposition and polymer removal treatment to release lithographic nanostructures. (c) Pattern transfer to SiO_2 hardmask and sacrificial carbon layer etching. (d) Carbon line trimming and SiO_2 hard mask stripping. (e) Conformal titanium dioxide spacer deposition using ALD. (f) Spacer etch back and strip of sacrificial carbon between spacers.

of the deposition process and etch properties of suitable materials for UV-NIL template fabrication is required in order to maintain critical dimensions [11–14].

Double patterning methods have been adopted in the interim [15, 16] to overcome resolution limitations by halving feature size and pitch [17–19]. Among the different double patterning techniques, spacer defined double patterning (SDDP) gains particular attention because it does not suffer from overlay issues and can achieve high throughputs [20, 21]. In SDDP (figure 1, progressing from steps (d)–(f)), a highly conformal spacer layer is deposited onto a sacrificial mandrel pattern. Next, the spacer is etched back and the mandrel removed, resulting in a patterned layer with narrow spacer features. The key element for a successful SDDP integration is the performance of the spacer technology. Atomic layer deposition (ALD) is particularly appropriate for the spacer fabrication [22, 23] because it produces excellent conformity and uniformity without loading effect across an entire wafer [21]. ALD allows the formation of ultra-thin films with angstrom-level resolution by cyclical oxidation of a metal–organic precursor [24, 25]. Control of the ALD parameters is instrumental in defining the feature size and frequency of the double patterned lines.

The ALD deposition step in SDDP must fulfill three main requirements for achieving single-digit nanometer accuracy. First, the oxide deposition must not damage the underlying materials. Second, nucleation and growth on different surfaces should promote the formation of either a uniformly thick film or a thinner film at the bottom of the trenches. An uneven film with less deposition at the bottom of the trench would balance the discrepancy in the etching rate between trench tops and bottoms (tops tend to etch faster than bottoms) [26]. Finally, the deposited material should have enough mechanical integrity to prevent line collapse when the mandrel is removed.

In this work, we focus on the ALD process used during SDDP. The ALD layer grows on two different materials: carbon, which defines the mandrel, and chromium, which defines the hard mask for future quartz etching (figure 1(e)). To begin this study we prepared flat substrates of carbon, chromium as well as silicon dioxide, which is used as a reference material. Using flat samples is imperative for the *in situ* spectroscopic ellipsometry (SE) to study the growth of the ALD layers. During the ALD of titanium dioxide (TiO_2) and silicon dioxide (SiO_2) we look at nucleation and etch properties to better understand the initial deposition phase. We show that the plasma processes using tris(dimethylamino) silane (TDMAS) as the SiO_2 precursor interacts with the carbon. TiO_2 worked with both plasma and thermal processes. However, thermal processes better maintained the integrity of the underlying carbon and chromium layer.

After defining a viable spacer deposition process with blanket samples, our patterning approach employs the use of self-assembled block copolymer lithography [27] in combination with SDDP [18] to reach the sub-10 nm regime (figure 1). Patel *et al* demonstrated the use of multi-patterning for pitch doubling from a starting lamellae polystyrene-*b*-poly (methyl methacrylate) (PS-*b*-PMMA) [28]. Here we use

PS-*b*-PMMA with 30 nm starting pitch. From previous research, we demonstrated nanoscale etching of relevant materials for imprint template fabrication at sub-10 nm dimensions [29–33]. We build on this experience to identify a material stack with coordinated selectivities for high resolution pattern transfer in the SDDP process. By using the results of the ALD study, we ultimately show the fabrication of ALD generated TiO_2 features on chromium with 7.5 nm width.

Materials and methods

For this work, two types of substrates were used: (1) flat substrates for ellipsometric analysis and (2) patterned structures for sub-10 nm features fabrication.

Flat substrates fabrication (1)

SiO_2 and TiO_2 were grown in a plasma-enhanced ALD reactor (Oxford Instruments FlexAL) on three types of flat substrates; thermal silicon dioxide (SiO_2), e-beam evaporated chromium (Cr) and sputtered carbon (spC). Carbon and chromium coated wafers were used to represent the carbon mandrel and chromium underlayer respectively, while SiO_2 was used as a reference material. Temperatures of 200 °C and 300 °C were used because these higher temperatures promote mechanical strength and reduce collapse after removing the mandrel [19, 34].

Nucleation and growth during ALD were studied *in situ* using SE (J A Woollam Co., Inc., M2000) fitted on the Oxford FlexAL ALD reactor. Under many conditions, SE can detect thickness changes in the submonolayer range [35]. Substrates were measured before ALD deposition to facilitate the optical modeling of the material film during growth. The optical constant of the ALD material was determined after 200 cycles and then used for modeling the film thickness.

Spacer defined pattern doubling for sub-10 nm features (2)

The process we considered for BPM master template fabrication is shown in figure 1. The process in total involves 6 dry etching steps, 1 wet etching step, and 2 deposition steps. All the steps involved in the SDDP have been properly developed in order to have stable and reproducible results and minimize time-to-time variations. Samples of $1 \times 1\ in^2$ were used during the optimization of the processes. Over these samples, the features were completely uniform.

Material stack. The material stack (provided by Seagate Technology LLC) is comprised of a 6″ prime grade silicon wafer substrate with 300 nm thermal SiO_2, 5 nm e-beam evaporated chromium, 20 nm sputtered carbon and a 7 nm SiO_2 layer. The unguided block copolymer film of PS-*b*-PMMA block copolymer had a full pitch of 30 nm.

Figure 1(a) → figure 1(b): sequential infiltration synthesis (SIS). In order to enhance the selectivity between the pattern formed by BCP and the underlying SiO_2, aluminum oxide was selectively synthesized in the PMMA domain by exposing the PS-*b*-PMMA film to TMA and water vapors [25, 36–40]. The infiltration was performed using an Ultratech/Cambridge NanoTech Savannah (S100) ALD system. The process temperature of 85 °C, is below the glass transition temperature of PS-*b*-PMMA BCP [41]. The precursors exposure was carried out at a pressure of 250 mTorr with a dosing time of 300 s. A study on TMA/water precursors exposure dependence on pressure and time is included in the supporting information, which is available online at stacks.iop.org/NANO/29/405302/mmedia.

Polymer removal. After selectively hardening the PMMA domain over PS, the BCP film was stripped by oxygen plasma in an Oxford Instruments 80+ reactive ion etcher (RIE) at 110 V DC bias and 20 °C to remove the remaining polymer and form infiltrated Al_xO_y lines (figure 1(b)).

(b) → (c): pattern transfer to SiO_2. A 7 nm SiO_2 layer is used under the BCP to promote a specific surface chemistry for graphoepitaxy [27]. The Al_xO_y lines are transferred to this SiO_2 layer using fluorine-based plasma. The etching was carried out in a multiple frequencies parallel plate tool (Oxford Instruments) with 60 MHz on the top plate and 13.56 MHz on the bottom plate. The chamber was filled with 80 sccm SF_6 at 20% O_2 and kept at 5 mTorr. We applied 150 W of radio frequency power and 400 W VHF forward power for 6 s. The resulting SiO_2 lines were used as a hard mask for etching the 20 nm sputtered carbon layer.

Carbon etch and trim. The Carbon was etched in an oxygen plasma at cryogenic temperature (−100 °C) in an Oxford Instruments PlasmaLab 100 (Cobra) inductively coupled plasma (ICP) system. The forward power was 20 W and ICP power was 1000 W. The flow rate of O_2 was 20 sccm, and chamber pressure was set to 6 mTorr (figure 1(c)). The width of the lines was controlled by the etching time. A 90 s etch time left a 15 nm line. Increasing the etching time to 270 s reduced the mandrel width to 8 nm.

(c) → (d): hard mask stripping. SiO_2 and Al_xO_y were removed by hydrofluoric acid dip (40% dilution) leaving carbon lines at 30 nm pitch and 8 nm width (figure 1(d)).

(d) → (e): titanium dioxide deposition. 7.5 nm thick TiO_2 film was conformally deposited on trimmed mandrel lines by thermal ALD (Oxford FlexAl) at 200 °C. The process used alternating steps of Tetrakis(dimethylamido) titanium (TDMAT) dosing and oxidation in which reactive oxygen was created from water vapor. TDMAT dosing was carried out at a pressure of 80 mTorr for a time of 800 ms, followed by a 6 s purging step. The oxidation step was then performed using water vapor at a pressure of 80 mTorr for 120 ms. The water dose was followed by 10 s purging step with 400 sccm argon gas flow.

(e) → (f): etch back. The planar surfaces on the bottom and the top of the deposited TiO_2 were etched back in a fluorine-based ICP-RIE. At 4 mTorr the flow rates CF_4 and O_2 were

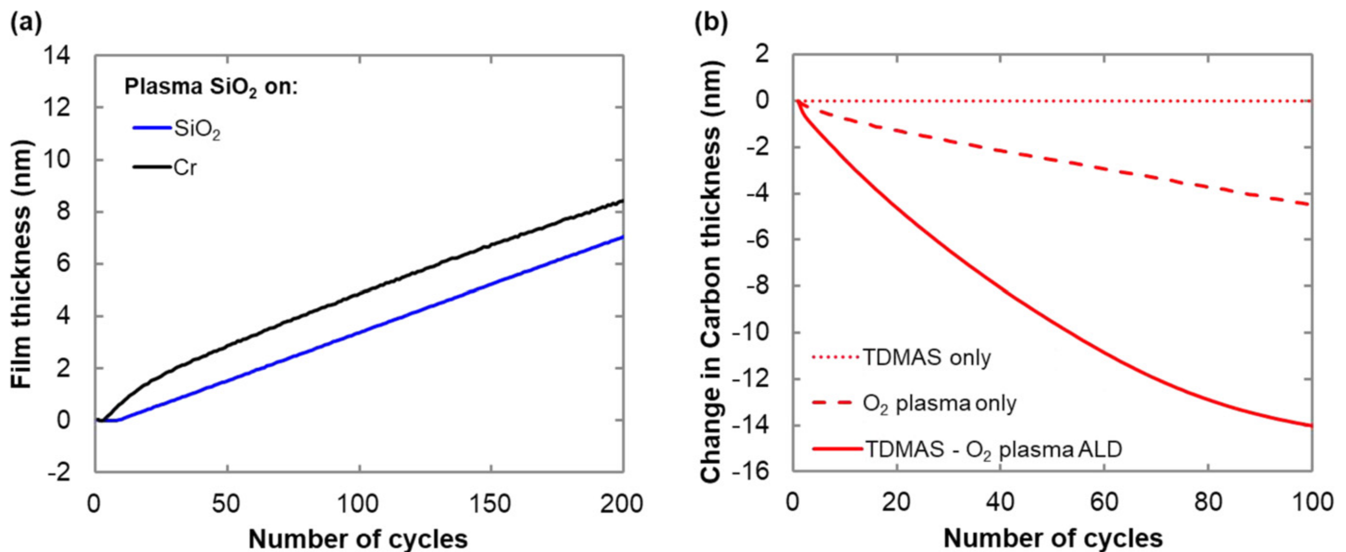

Figure 2. (a) ALD growth of plasma SiO_2 at 300 °C on two substrates: thermal SiO_2 and chromium (Cr). (b) Changes in carbon thickness during plasma SiO_2 ALD deposition at 300 °C (continuous line), O_2 plasma exposure step alone (dashed line), and TDMAS injection step alone (dotted line).

33 sccm and 3 sccm respectively. Etching was done for 45 s at 25 W RF power and 180 W ICP power. After etching, the height of the features was reduced to 8 nm.

Carbon strip. The carbon mandrel was removed by O_2 plasma at 20 °C in an ICP-RIE at low forward power of 2 W RF with 1 V DC bias to prevent damage to the TiO_2 lines. Process conditions had an oxygen flow of 8 sccm, pressure 5 mTorr, ICP power of 250 W and 75 s etch time.

Results and discussion

ALD growth on flat substrates

Silicon dioxide deposition was tested both thermally and with plasma on flat substrates (1), using tris(dimethylamino)silane (TDMAS) as a precursor. However, surface species deposited by TDMAS were found to be unreactive using water vapor at temperatures ranging from 40 °C to 300 °C. After 200 cycles of thermal SiO_2 ALD, no material was detected on the surface by *in situ* SE analysis. This result is consistent with the previous finding of Burton and Kang [42]. SE measurements show SiO_2 thin films deposits from TDMAS and O_2 plasma at 300 °C on silicon dioxide and chromium with a growth rate of 0.036 ± 0.005 nm/cycle (figure 2(a)). The initial growth rate of SiO_2 on chromium is higher than SiO_2 on SiO_2 due to the formation of chromium oxide which results in an apparent increase in thickness. Notably, plasma SiO_2 deposition on sputtered carbon produced unexpected results. After 100 cycles SiO_2 plasma-enhanced ALD, the carbon layer was no longer present (figure 2(b)—TDMAS-O_2 plasma ALD). We initially hypothesized that the plasma etching step removed the carbon. However, we found that running a continuous oxygen plasma step with the same process condition used in ALD oxygen step (figure 2(b)—O_2 plasma only) produced a carbon etch rate much slower than the etch rates we observed during the full ALD sequence. The ALD precursor exposure step run alone was not found to remove any carbon (figure 2(b)—TDMAS only). Presumably, there is a synergistic reaction between the SiO_2 precursor and carbon that promotes faster removal in an oxygen plasma. Overall we did not find a suitable thermal or plasma ALD process using the TDMAS precursor for deposition of SiO_2. We subsequently found success investigating the TiO_2 ALD process.

Titanium oxide ALD films were deposited from Tetrakis (dimethylamido)titanium (TDMAT) metal–organic precursor on sample type (1) using both thermal and plasma processes. To minimize line edge roughness due to crystallinity, we performed TiO_2 growth at temperatures below 250 °C where the formation of large crystallites is minimized [43–45].

Unlike our SiO_2 precursor, TDMAT works in both thermal and plasma-based processes and we were thus able to evaluate both. Figure 3(a) shows the nucleation behavior of thermal and plasma TiO_2 ALD at 200 °C on the three different substrates: chromium, carbon, and silicon dioxide. Nucleation behavior of the films on these substrates is shown in figure 3(b). While the growth rates of thermal and plasma ALD are not significantly different, 0.042 ± 0.005 nm/cycle for thermal versus 0.052 ± 0.005 nm/cycle for plasma, the nucleation behavior is different. As observed in the plasma growth of SiO_2 on chromium, the nucleation of TiO_2 shows a higher slope. This behavior is absent in the thermal growth. We hypothesized that oxygen plasma promotes an apparent change in thickness due to the formation of chromium oxide. This conclusion is confirmed in the work of Langereis *et al* [44], where they show an initial accelerated growth during plasma ALD on different substrates. When plasma TiO_2 grows on carbon, measured film thickness first drops below zero and then increases to reach a constant growth rate. We believe the carbon is etched during the nucleation phase, the first few cycles, and then the carbon surface is passivated with

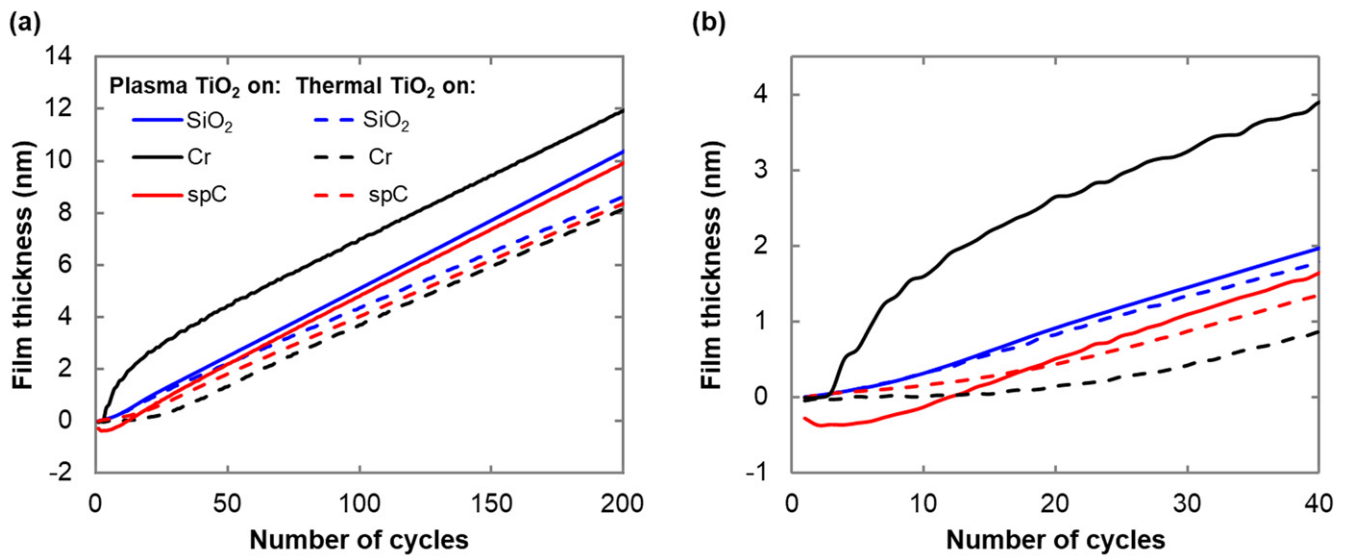

Figure 3. (a) TiO_2 layer thickness measured by *in situ* SE as a function of the number of ALD cycles at 200 °C on different substrates: thermal silicon oxide (SiO_2-blue), carbon (spC-red), chromium (Cr-black). Titanium dioxide ALD alternated TDMAT dosing and oxidation where oxygen is given by water vapor (dashed line) and O_2 plasma (continuous line). Graph (b) represents a zoom of the first 40 cycles of the deposition, showing the nucleation behavior.

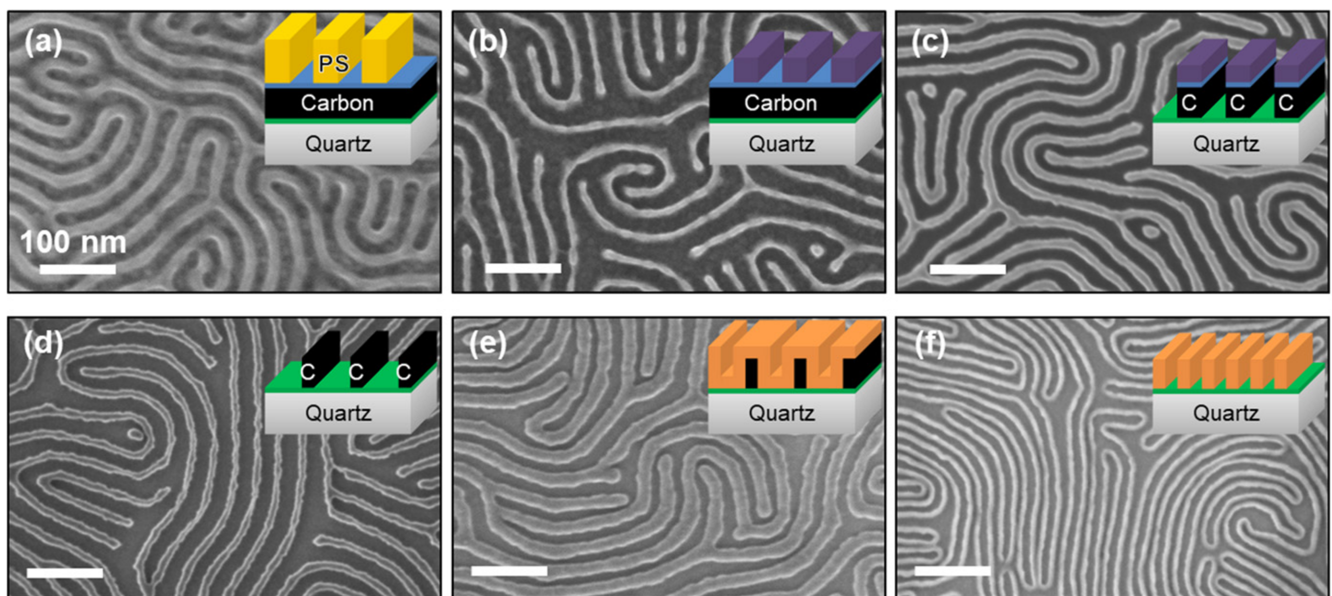

Figure 4. Top view SEM images of unguided BCP line doubling pattern transfer demonstration corresponding to the schematic process flow in the inset. (a) Self-assembly of PS-*b*-PMMA BCP with 30 nm pitch after stripping the PMMA. (b) Pattern after selective sequential infiltration synthesis of Al_xO_y in the PMMA domain and polymer removal. (c) Pattern transferred to SiO_2 and carbon mandrel. (d) 30 nm pitch, 7.5 nm wide carbon mandrel lines. (e) Conformal thermal ALD of TiO_2 spacer over mandrel features. (f) 15 nm pitch spacer lines after etching and mandrel removal.

the first layers of TiO_2. Note, however, that when carbon is used as a mandrel in the patterning process, any etching can be detrimental for sub-10 nm dimensions. Therefore, in order to minimize damage to the substrate and to avoid any etching, oxidation or acceleration during the growth, we decided to move away from any O_2 plasma activated process.

Nucleation of thermal TiO_2 on the three substrates does not show any etching, and a delay is observed on chromium. This delay is small and unlikely to result in a significant process benefit (reduced ALD thickness at the trench bottoms to counteract reduced etch rates) [26]. Overall, the TiO_2 thermal process was the best process identified and used as the ALD step in our SDDP process.

Demonstration of 7.5 nm half-pitch TiO_2 features via SDDP

Figure 4 shows selected key steps of the full pattern doubling process in a top down view. The selective infiltration process was optimized to create an initial pattern of 15 nm (PS-*b*-PMMA half-pitch) after infiltration and polymer removal

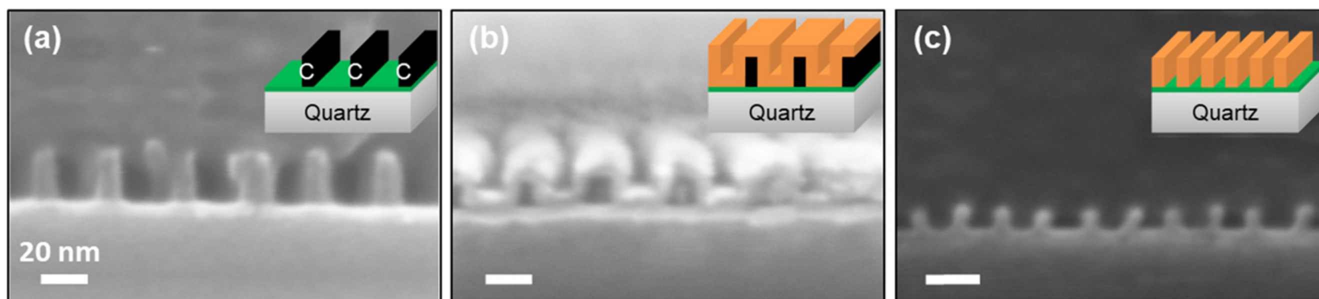

Figure 5. (a)–(c) Cross-sectional view SEM images of the double patterning steps corresponding to the schematic in the top right corner. (a) 30 nm pitch sputtered carbon mandrel lines. (b) Conformal thermal ALD TiO_2 spacer deposition over 8 nm carbon mandrel features. (c) 7.5 nm pitch TiO_2 lines after SDDP.

(figure 4(b)) (see supporting information). This pattern is etched into the oxide layer and then the carbon (figure 4(c)). After the carbon trim step and mask removal, figure 4(d) shows an increase in edge roughness in the top down image. However, we found that subsequent process seemed to smooth the sidewalls. Next, TiO_2 was deposited by ALD, using the thermal deposition process at 200 °C. This ALD layer was etched to produce titanium features at 7.5 nm half-pitch (figure 4(e)).

Figure 5 shows a cross-sectional view of the last three steps in the double patterning process. Where figure 5(a) shows 30 nm pitch carbon mandrel lines fabricated using PS-*b*-PMMA block copolymer along with SIS pattern transfer. Figure 5(b) shows the resulting 7.5 nm conformal TiO_2 spacer deposited on the carbon mandrel. After back etching the TiO_2 using CF_4 at 10% O_2 in an inductively coupled plasma reactor, figure 5(c) shows resulting features with 7.5 nm half-pitch. ICP power of 180 W and RF of 25 W etch 7.5 nm TiO_2 in 30 s. In order to etch through TiO_2 at the bottom of the trenches, a longer etching time is used. This leaves TiO_2 features with a height of 8 nm (after mandrel removal using standard oxygen plasma) (figure 5(c)). TiO_2 is a high selectivity mask for the subsequent chromium patterning step so this height is sufficient to pattern the underlying chromium. Note, that some lines in figure 5(c) appear tilted. This is not due to pattern collapse but rather an artifact of the conformal coating of the carbon mandrel. During the oxygen etching and trimming of carbon features, carbon structures develop a widened footing portion at their base (figure 5(a)). After etching the TiO_2 layer, the remaining feature conforms to the tilt of the carbon pattern. We are currently tuning the carbon etching to reduce this effect. The TiO_2 structures in figure 5(c) could be used directly as the structural template material, or alternatively transferred to the underlying chromium layer using chlorine and oxygen gas mixture plasma [30].

Conclusions

We were able to fabricate sub-10 nm half-pitch pattern through a combination of self-assembled block copolymer and SDDP. In this work we demonstrated the fabrication of 15 nm carbon lines using selective infiltration by ALD of PS-*b*-PMMA block polymer. Using SE, we conducted detailed studies of the deposition of the spacer on flat substrates, chromium and carbon, as a function of the number of ALD cycles. After studying SiO_2 and TiO_2 processes, both plasma and thermal, we chose a thermal TiO_2 process. SiO_2 could only be deposited by plasma and ended up etching the carbon. We demonstrated the etching process was due to a synergistic reaction between the ALD precursor and the O_2 plasma; O_2 plasma alone etched the carbon considerably slower. Carbon was more stable in the TiO_2 plasma process but underwent some etching. In addition, it appeared that plasma processes promoted the growth of chromium oxide. We thus moved to a thermal TiO_2 process for SDDP demonstration which did not damage the mandrel and ends with 7.5 nm robust standing lines that are not subject to pattern collapse. However, the lines did exhibit a slight tilt. To minimize this tilt, the carbon trim will need to be optimized to reducing any footing at the bottom of the feature.

Overall, using SDDP fabrication approach we proposed a systematic route to enable sub-10 nm feature size transfer over large areas. Notably, it is possible to take advantage of the wafer stack and extend the implementation of this method using substrates compatible to chromium deposition. This type of process enables scalable fabrication of single digit nanometer feature sizes for both patterned media at densities beyond 5 Tb/in^2 and integrated circuits. The next steps in BPM master template fabrication are to transfer the TiO_2 pattern into the underlying chromium and then into the quartz template. This will be demonstrated in subsequent work.

Acknowledgments

This work was completed at the Molecular Foundry and supported by the Office of Science, Office of Basic Energy Sciences, of the US Department of Energy under Contract No. DE-AC02-05CH11231. We are especially grateful to Oxford Instruments for support of SD. Further we thank Seagate Technology LLC for support of DS. These authors would like to thank Simone Sassolini, Michael Elowson and Hilary Brunner for their support.

ORCID iDs

Stefano Dallorto https://orcid.org/0000-0002-4072-4543

References

[1] Yang X *et al* 2009 Directed block copolymer assembly versus electron beam lithography for bit-patterned media with areal density of 1 Terabit/inch^2 and beyond *ACS Nano* **3** 1844–58
[2] Chou S Y 1997 Patterned magnetic nanostructures and quantized magnetic disks *Proc. IEEE* **85** 652–71
[3] Thompson D A and Best J S 2000 The future of magnetic data storage techology *IBM J. Res. Dev.* **44** 311–22
[4] Yang X *et al* 2007 Challenges in 1 Teradot/in 2 dot patterning using electron beam lithography for bit-patterned media *J. Vac. Sci. Technol.* B **25** 2202–9
[5] Okazaki S 1991 Resolution limits of optical lithography *J. Vac. Sci. Technol.* B **9** 2829–33
[6] Manfrinato V R *et al* 2013 Resolution limits of electron-beam lithography toward the atomic scale *Nano Lett.* **13** 1555–8
[7] Dobisz E A *et al* 2008 Patterned media: nanofabrication challenges of future disk drives *Proc. IEEE* **96** 1836–46
[8] Ruiz R, Dobisz E and Albrecht T R 2010 Rectangular patterns using block copolymer directed assembly for high bit aspect ratio patterned media *ACS Nano* **5** 79–84
[9] Austin M D *et al* 2004 Fabrication of 5 nm linewidth and 14 nm pitch features by nanoimprint lithography *Appl. Phys. Lett.* **84** 5299–301
[10] Peroz C *et al* 2011 Single digit nanofabrication by step-and-repeat nanoimprint lithography *Nanotechnology* **23** 015305
[11] Albrecht T R *et al* 2015 Bit-patterned magnetic recording: theory, media fabrication, and recording performance *IEEE Trans. Magn.* **51** 1–42
[12] Kuhn K J *et al* 2011 Process technology variation *IEEE Trans. Electron Devices* **58** 2197–208
[13] Lee C G, Kanarik K J and Gottscho R A 2014 The grand challenges of plasma etching: a manufacturing perspective *J. Phys. D: Appl. Phys.* **47** 273001
[14] Donnelly V M and Kornblit A 2013 Plasma etching: yesterday, today, and tomorrow *J. Vac. Sci. Technol.* A **31** 050825
[15] Owa S *et al* 2006 Current status and future prospect of immersion lithography *SPIE 31st Int. Symp. on Advanced Lithography* (SPIE)
[16] Borodovsky Y 2006 Marching to the beat of Moore's Law *SPIE 31st Int. Symp. on Advanced Lithography* (SPIE)
[17] Raley A 2016 A spacer-on-spacer scheme for self-aligned multiple patterning and integration *SPIE Newsroom* https://doi.org/10.1117/2.1201608.006583
[18] Yu Z *et al* 2001 Fabrication of large area 100 nm pitch grating by spatial frequency doubling and nanoimprint lithography for subwavelength optical applications *J. Vac. Sci. Technol.* B **19** 2816–9
[19] Dhuey S *et al* 2013 Obtaining nanoimprint template gratings with 10 nm half-pitch by atomic layer deposition enabled spacer double patterning *Nanotechnology* **24** 105303
[20] Beynet J *et al* 2009 Low temperature plasma-enhanced ALD enables cost-effective spacer defined double patterning (SDDP) *SPIE Lithography Asia* (SPIE)
[21] Profijt H *et al* 2011 Plasma-assisted atomic layer deposition: basics, opportunities, and challenges *J. Vac. Sci. Technol.* A **29** 050801
[22] Beynet J *et al* 2009 Low temperature plasma-enhanced ALD enables cost-effective spacer defined double patterning (SDDP) *Lithography Asia 2009* (International Society for Optics and Photonics)
[23] Bak C H *et al* 2015 Ultrahigh density sub-10 nm TiO_2 nanosheet arrays with high aspect ratios via the spacer-defined double-patterning process *Polymer* **60** 267–73
[24] Mackus A, Bol A and Kessels W 2014 The use of atomic layer deposition in advanced nanopatterning *Nanoscale* **6** 10941–60
[25] Moon H S *et al* 2014 Atomic layer deposition assisted pattern multiplication of block copolymer lithography for 5 nm scale nanopatterning *Adv. Funct. Mater.* **24** 4343–8
[26] Gottscho R A, Jurgensen C W and Vitkavage D 1992 Microscopic uniformity in plasma etching *J. Vac. Sci. Technol.* B **10** 2133–47
[27] Griffiths R A *et al* 2013 Directed self-assembly of block copolymers for use in bit patterned media fabrication *J. Phys. D: Appl. Phys.* **46** 503001
[28] Patel K *et al* 2012 Line-frequency doubling of directed self-assembly patterns for single-digit bit pattern media lithography *Pro. SPIE* **8323** 83230U
[29] Liu Z *et al* 2012 Super-selective cryogenic etching for sub-10 nm features *Nanotechnology* **24** 015305
[30] Staaks D *et al* 2016 Low temperature dry etching of chromium towards control at sub-5 nm dimensions *Nanotechnology* **27** 415302
[31] Olynick D L, Liddle J A and Rangelow I W 2005 Profile evolution of Cr masked features undergoing HBr-inductively coupled plasma etching for use in 25nm silicon nanoimprint templates *J. Vac. Sci. Technol.* B **23** 2073–7
[32] Welch C C *et al* 2013 Formation of nanoscale structures by inductively coupled plasma etching *Int. Conf. on Micro-and Nano-Electronics 2012* (International Society for Optics and Photonics)
[33] Gu X *et al* 2012 High aspect ratio sub-15 nm silicon trenches from block copolymer templates *Adv. Mater.* **24** 5688–94
[34] Van Hemmen J *et al* 2007 Plasma and thermal ALD of Al_2O_3 in a commercial 200 mm ALD reactor *J. Electrochem. Soc.* **154** G165–9
[35] Tompkins H and Irene E A 2005 *Handbook of Ellipsometry* (Norwich, NY: Elsevier)
[36] Peng Q *et al* 2010 Nanoscopic patterned materials with tunable dimensions via atomic layer deposition on block copolymers *Adv. Mater.* **22** 5129–33
[37] Tseng Y-C *et al* 2011 Etch properties of resists modified by sequential infiltration synthesis *J. Vac. Sci. Technol.* B **29** 06FG01
[38] Ruiz R *et al* 2012 Image quality and pattern transfer in directed self assembly with block-selective atomic layer deposition *J. Vac. Sci. Technol.* B **30** 06F202
[39] Tseng Y-C *et al* 2011 Enhanced polymeric lithography resists via sequential infiltration synthesis *J. Mater. Chem.* **21** 11722–5
[40] Tseng Y-C *et al* 2011 Enhanced block copolymer lithography using sequential infiltration synthesis *J. Phys. Chem.* C **115** 17725–9
[41] Ramanathan M *et al* 2013 Emerging trends in metal-containing block copolymers: synthesis, self-assembly, and nanomanufacturing applications *J. Mater. Chem.* C **1** 2080–91
[42] Burton B *et al* 2009 SiO_2 atomic layer deposition using tris (dimethylamino) silane and hydrogen peroxide studied by *in situ* transmission FTIR spectroscopy *J. Phys. Chem.* C **113** 8249–57
[43] Abendroth B *et al* 2013 Atomic layer deposition of TiO_2 from tetrakis (dimethylamino) titanium and H_2O *Thin Solid Films* **545** 176–82
[44] Langereis E *et al* 2009 *In situ* spectroscopic ellipsometry as a versatile tool for studying atomic layer deposition *J. Phys. D: Appl. Phys.* **42** 073001
[45] Mitchell D *et al* 2005 Atomic layer deposition of TiO_2 and Al_2O_3 thin films and nanolaminates *Smart Mater. Struct.* **15** S57